THE JOURNAL OF PHYSICAL CHEMISTRY C
A JOURNAL OF THE AMERICAN CHEMICAL SOCIETY

pubs.acs.org/JPCC

Article

Salts Induce Enhanced Disintegration of Natural Minerals in Charged Water Microdroplets

Jamshiya Sulthana,[‖] Anubhav Mahapatra,[‖] Mridula Bhan, Depanjan Sarkar,* and Thalappil Pradeep*

Cite This: https://doi.org/10.1021/acs.jpcc.6c00820

Read Online

ACCESS | Metrics & More | Article Recommendations | Supporting Information

ABSTRACT: Charged water microdroplets have been demonstrated to be microreactors capable of disintegrating hard minerals into nanoparticles (NPs) under ambient conditions. However, the high applied potentials required (~4−4.5 kV) limit the energy efficiency and industrial applications of the phenomenon. Herein, we demonstrate that when aqueous solutions containing trace concentrations of salts (0.1 ppm) are electrosprayed, the threshold potential for quartz disintegration decreases by up to 85%, leading to the formation of 2−10 nm NPs at voltages as low as 1.5 kV. Systematic variation in salt concentration reveals that enhanced droplet conductivity, surface tension, interfacial charge polarization, and localized electric field amplification collectively facilitate efficient disintegration at lower voltages. The effect of ionic size was systematically investigated through different cations (H^+ to Cs^+) and anions (F^- to I^-), establishing that smaller ions promote stronger field localization and faster charge relaxation dynamics. COMSOL simulations elucidate how ionic additives modulate droplet deformation and cleavage of the mineral lattice. This salt-assisted electrospray route offers a green, energy-efficient, and scalable strategy for the ambient synthesis of mineral-derived nanomaterials.

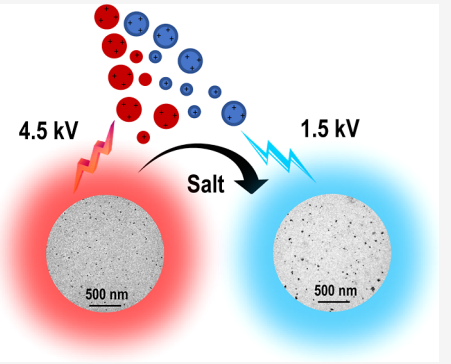

INTRODUCTION

Mineral disintegration is an energy-intensive process because naturally occurring minerals are mechanically robust and chemically inert. Conventional methods such as mechanical grinding, high-temperature oxidation, and acid leaching require substantial energy inputs[1] and often generate environmental waste,[2] making them unsustainable for large-scale or eco-friendly applications.[3] Developing alternative methods that achieve mineral breakdown efficiently under mild conditions remains a major scientific and technological challenge. In recent years, charged microdroplets have emerged as unique microreactors that enable chemical transformations distinct from those in bulk solutions.[4−6] Within these confined, charged environments, reactions proceed at remarkably enhanced rates due to strong interfacial electric fields,[7] the generation of reactive species, and nonequilibrium conditions.[8,9] These unusual physicochemical features have allowed a range of ambient chemical reactions to occur rapidly and with minimal energy input, revealing a new dimension of green chemistry. Beyond facilitating chemical reactions, our group has also reported pioneering work on synthesizing nanomaterials using charged microdroplets, thereby extending their utility from reaction media to platforms for material fabrication.[10−14]

Building on these advances, our group has recently demonstrated that charged water microdroplets can disintegrate natural minerals into nanoparticles (NPs) under ambient conditions.[15,16] This microdroplet-based mineral disintegration process is referred to as microdroplet mechanochemistry.[17] Using electrospray-generated droplets, we observed that minerals undergo spontaneous fragmentation during droplet flight, driven by the combined effects of interfacial charge density, electric field-induced stress, and hydrodynamic deformation. This discovery establishes microdroplet chemistry as a sustainable pathway to convert solid minerals into functional nanomaterials with potential applications in catalysis, environmental remediation, and beyond.[18] Although this fascinating research has opened many exciting possibilities, two major limitations remain for practical relevance: the high operational potential required for effective mineral disintegration (≥4−4.5 kV) and the reliance on high purity water, which reduces the overall cost-effectiveness of the process. In natural aqueous environments, minerals coexist with dissolved salts. Ionic additives modulate droplet conductivity and interfacial charge dynamics, influencing the droplet stability and local electric field intensity.

In this study, we demonstrate that introducing trace concentrations of salts (0.1 ppm) into water significantly reduces the threshold potential for quartz disintegration by up to 85%, resulting in the formation of 2−10 nm NPs at voltages as low as 1.5 kV. Systematic investigation at varying salt

Received: February 5, 2026
Revised: March 11, 2026
Accepted: March 16, 2026

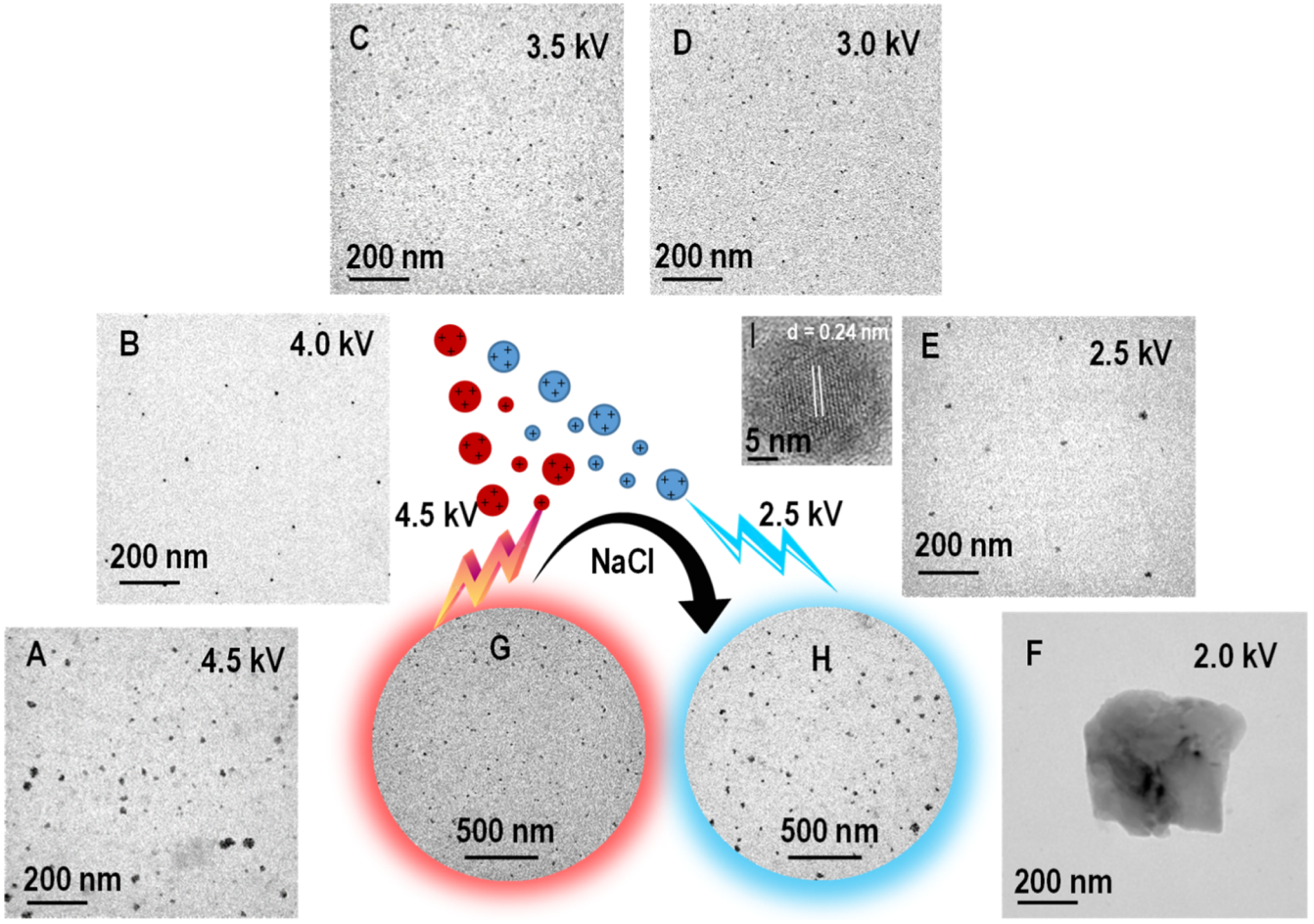

Figure 1. Disintegration of quartz particles in water containing 0.5 ppm of NaCl under varied electrospray conditions. (A–F) TEM images of quartz particles obtained after electrospray at applied potentials ranging from 4.5 to 2.0 kV, with a tip-to-substrate distance of 1.5 cm. TEM images without NaCl (G) and with (H) NaCl showing that even trace amounts of salt markedly enhanced the disintegration efficiency by reducing the required applied voltage from 4.5 to 2.5 kV (by 55%). (I) HRTEM image of an individual quartz NP showing distinct lattice fringes with an interplanar spacing of 0.24 nm, corresponding to the (110) plane of quartz.

concentrations and ionic sizes, ranging from H^+ to Cs^+ for cations and F^- to I^- for anions, showed that smaller, more mobile ions induce stronger interfacial polarization and localized field amplification. COMSOL simulations further elucidate how the addition of a trace amount of salt promotes efficient droplet deformation and mineral lattice cleavage. This work establishes a mechanistic framework for ion-assisted mineral disintegration in charged water microdroplets, emphasizing that salts are not only additives but also naturally occurring species that fundamentally influence microdroplet mechanochemistry. The findings highlight a green, energy-efficient, and scalable strategy for the ambient synthesis of mineral-derived nanomaterials inspired by natural processes.

EXPERIMENTAL SECTION

Experimental details are presented in the Supporting Information. Briefly, locally sourced quartz (river sand) was ground and purified, and the size was selected by centrifugation as described therein. For all the experiments, particles of 5–10 μm size (Figure S1) were suspended in ultrapure Milli-Q water (18 MΩ·cm) containing various concentrations of NaCl (0.05–5 ppm, 0.86 μM–85.6 μM) depending on the experimental needs, followed by electrospray deposition (ESD) using a polyimide-coated fused silica capillary (ID = 50 μm) at an applied potential ranging from 1.5 to 4.5 kV and a fixed tip-to-substrate distance of 1.5 cm. Experimental techniques are presented in the Supporting Information, Sections S1, S2, and S3, and illustrated in Supporting Information, Figure S2.

RESULTS AND DISCUSSION

Initially, to optimize the required salt concentrations, NPs generated by ESD of aqueous suspensions of quartz, containing 0.5 ppm of NaCl, were systematically characterized using transmission electron microscopy (TEM), as depicted in Figure 1. Figure 1A–E illustrates the morphology of NPs formed under a decreasing applied potential ranging from 4.5 to 2.5 kV. These TEM images confirm the efficient and energy saving disintegration of quartz within this voltage range. Notably, at an applied potential of 2.0 kV (Figure 1F), the formation of predominantly larger aggregates was observed, indicative of incomplete disintegration and establishing a critical lower threshold for effective NP synthesis. Large-area TEM images acquired at 4.5 and 2.5 kV (Figure 1G,H, respectively) further confirm the consistent production of NPs with a narrow size distribution, ranging from 2 to 10 nm. High-resolution TEM (HRTEM) analysis (Figure 1I) reveals lattice fringes with a spacing of 0.24 nm, corresponding to the (110) c plane of quartz, thereby confirming the NPs. The starting material used for the ESD was quartz particles of sizes ranging from 5 to 10 μm, as verified by field emission scanning electron microscopy (Figure

https://doi.org/10.1021/acs.jpcc.6c00820
J. Phys. Chem. C XXXX, XXX, XXX–XXX

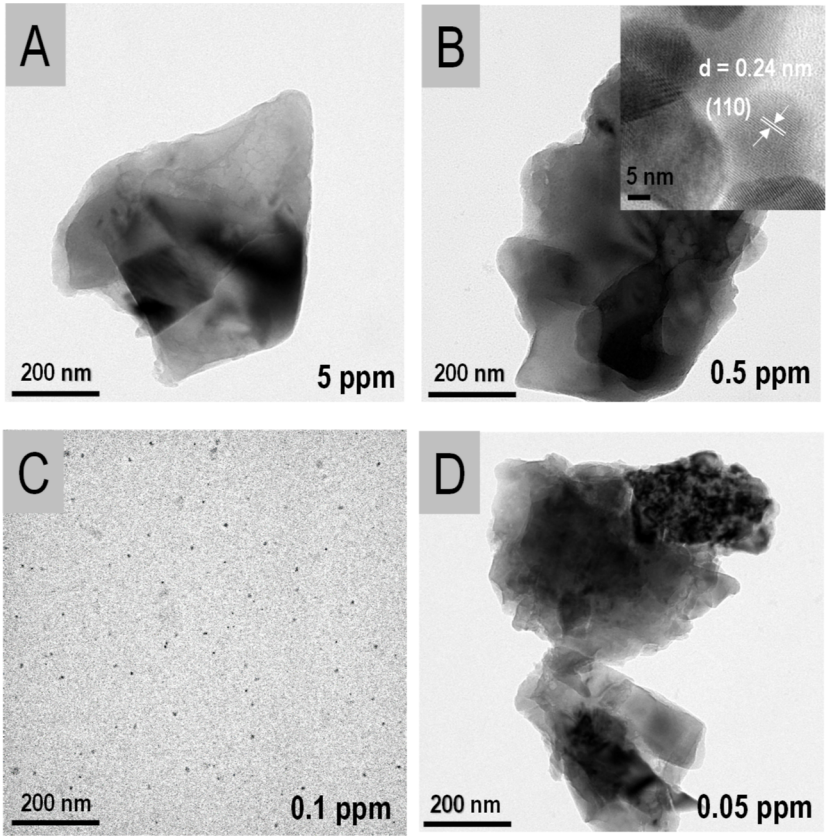

Figure 2. Disintegration of quartz particles in NaCl solution. (A–D) TEM images of quartz after electrospray of quartz suspension in different concentrations of NaCl: 5, 0.5, 0.1, and 0.05 ppm, respectively, at an applied potential of 2.0 kV, with a tip-to-substrate distance of 1.5 cm. HRTEM image of a particle is shown in the inset of B. The lattice plane shown is (110) of quartz.

S1), confirming the substantial size reduction achieved after post-ESD.

In control experiments conducted in the absence of salt, quartz disintegration was initiated only at applied potentials exceeding 4.5 kV, producing NPs within the 5–10 nm size range,[1,2] which aligns with the previous observations. The introduction of 0.5 ppm (8.56 μM) NaCl lowered this voltage threshold to 2.5 kV, reflecting a significant reduction of approximately 55% in the energy input required.

However, voltages below 2.0 kV resulted in incomplete mineral disintegration characterized by the formation of aggregates. Through systematic optimization, an optimal NaCl concentration of 0.1 ppm (1.71 μM) was identified, effectively balancing solution conductivity and surface tension parameters, as corroborated by theoretical analyses (explained in detail later).

Collectively, these findings demonstrate that the addition of traces of common salt markedly enhances the efficiency of quartz disintegration in charged microdroplets at substantially reduced applied voltages.

To identify the optimum NaCl concentration, ESD experiments were conducted at an applied voltage of 2.0 kV and a fixed tip-to-substrate distance of 1.5 cm, with varying NaCl concentration from 0.05 ppm (0.86 μM) to 5 ppm (85.6 μM), and the resulting products were analyzed by TEM (Figure 2A–D). At very low salt concentrations ($\leq$0.05 ppm), the ionic strength remained too low to support efficient charge transport, causing the droplets to behave similarly to ultrapure water and yield larger aggregates. In contrast, at higher concentrations ($\geq$0.5 ppm), increased surface tension, combined with stronger ion–solvent interactions, raises the energy barrier for droplet fission, compromising stability and promoting aggregation.

Thus, an intermediate concentration of 0.1 ppm of NaCl optimally balances solution conductivity and surface tension, thereby enabling efficient formation of well-dispersed quartz NPs upon ESD. This finding complements the potential dependent disintegration efficiencies described in Figure 1 and highlights the crucial interplay between ionic concentration and electrohydrodynamic parameters in modulating mineral fragmentation.

Cation Effects

Nature of the ion has a significant influence on both the energy efficiency of quartz disintegration and the morphology of the resulting NPs. To investigate this, we studied a series of alkali metal chlorides (LiCl to CsCl) and observed systematic variations in NP size, which correlated inversely with solution conductivity and directly with the cation radius. Small, strongly hydrated cations such as Li^+ promote efficient charge relaxation and field localization at the highly curved droplet interface under the experimental conditions (dilute salt concentrations ~1.5 μM), outweighing their lower bulk mobility (LiCl < NaCl < KCl). This results in more efficient droplet deformation and fragmentation, facilitating the formation of uniform quartz NPs at an applied potential of 1.5 kV (Figure 3). HCl showed enhanced comparable efficiency, producing NPs at applied potential as low as 1.5 kV, indicating that the proton-induced slip of the lattice has a role in mineral disintegration, further lowering the energy barrier. In contrast, larger alkali cations such as Na^+ to Cs^+ produced distinctly different effects. These ions induced

https://doi.org/10.1021/acs.jpcc.6c00820
J. Phys. Chem. C XXXX, XXX, XXX–XXX

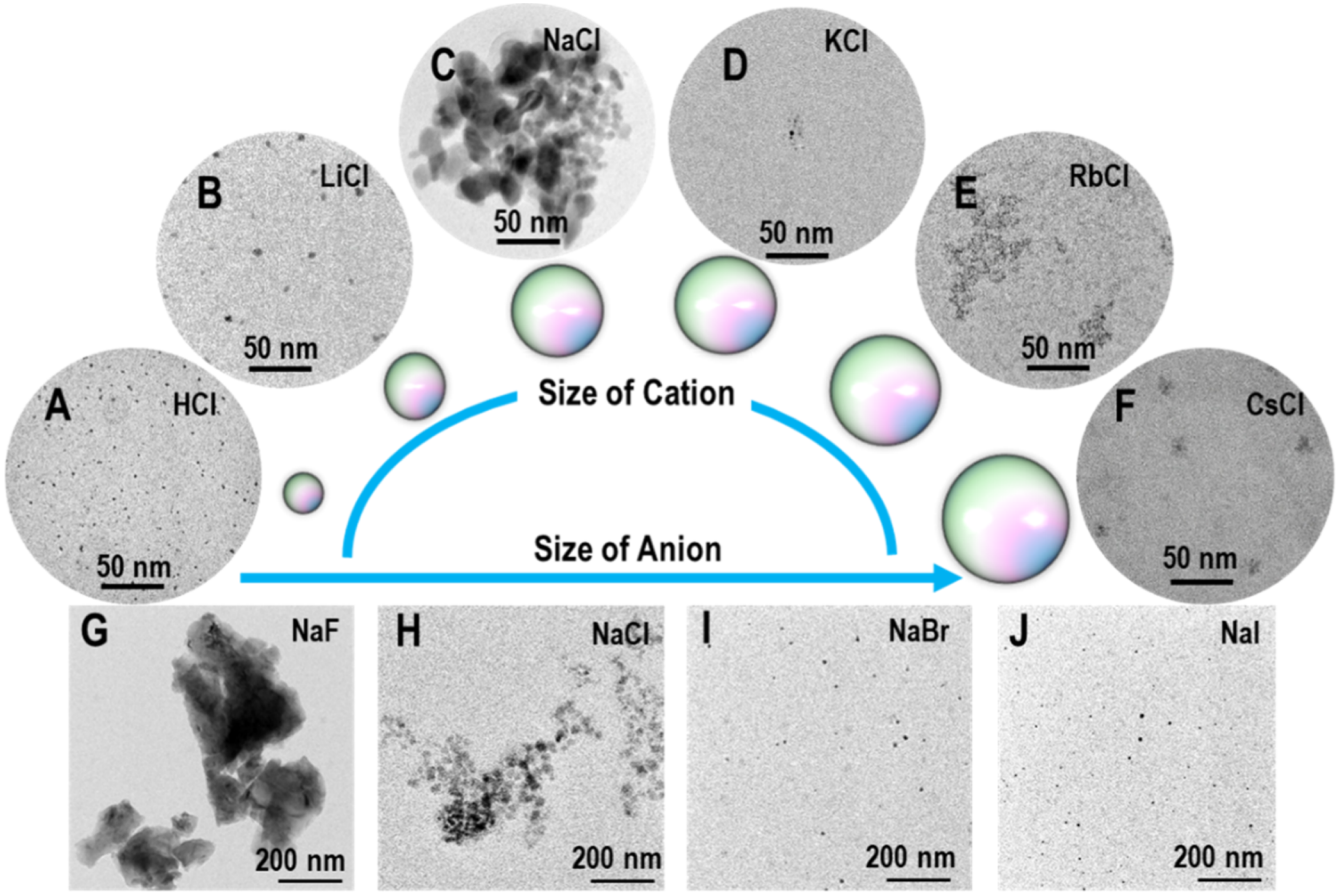

Figure 3. Disintegration of quartz particles in charged water microdroplets containing acid (HCl) and salt solutions at ppm levels. (A−F) TEM images showing morphological variations of quartz particles (suspended in different alkali metal chloride solutions) after electrospray at an applied potential of 2.0 kV, with a tip-to-substrate distance of 1.5 cm and a salt concentration of 0.1 ppm. (G−J) TEM images of quartz particles suspended in different sodium halide solutions (NaF, NaCl, NaBr, and NaI, respectively) following electrospray under identical conditions (2.0 kV, 1.5 cm, 0.1 ppm). Distinct morphological features highlight the influence of ionic composition on disintegration efficiency and particle transformation behavior.

anisotropic NP morphologies and aggregated structures (Figure 3C−F). We speculate that anisotropic morphologies and aggregated structures with larger cations (Na^+, Cs^+) are associated with cation bridging interactions in which weakly hydrated cations promote interparticle linkage and directional growth. These ions, having weaker hydration shells, adsorb directly onto negatively charged silanol sites ($Si{-}O^-$) on silica surfaces, forming shared bridges between NPs. Cs^+ neutralizes surface charge at lower concentrations than Li^+, enabling aggregation. These morphological effects underscore how ion hydration dynamics influence droplet stability and particle fragmentation pathways during ESD. Equal ion concentrations (1.5 μM HCl and NaCl) showed that ion type, not ionic strength, controls disintegration. H^+ enabled lower voltage disintegration due to proton-driven interfacial effects, whereas Na^+ required higher fields, confirming that the interfacial chemistry dictates energy efficiency. Detailed mechanistic explanations regarding the pathways of salt-assisted quartz disintegration, including the impact of equal ionic concentrations on electrohydrodynamic behavior and interfacial charge distribution, are provided in Supporting Information Section S5.2, supported by Figures S3 and S4.

In classical electrical double-layer models at planar interfaces, more weakly hydrated alkali cations (e.g., K^+, Na^+) form a compact Stern layer than strongly hydrated Li^+ at the same bulk concentration, leading to enhanced counterion accumulation and a reduced barrier to interfacial charge transfer. In our disintegration process, however, as droplets undergo strong curvature and rapid deformation, the effectiveness of a given cation is controlled by a competition between Stern-layer compactness and the rates of charge transport and relaxation in the bulk solution. Under our experimental conditions, LiCl solutions exhibit more favorable charge transport and relaxation characteristics than NaCl and KCl, enabling more efficient delivery of charge to the highly curved droplet apex and stronger local-field localization, which lower the disintegration voltage and favor the formation of uniform NPs.

Energy Efficiency Analysis

LiCl (1.5 μM) enables stable quartz disintegration at 1.5 vs 4.5 kV for pure water (Figure 3), suggesting substantial power savings. Using the measured spray currents and applied potentials, the following table (see Table 1) demonstrates the power requirement for the disintegration process. This

Table 1. Comparison of Power Consumption under Different Conditions

condition	applied voltage (kV)	spray current (μA)	power (mW)
pure water	4.5	0.85	3.83
NaCl	3.0	0.65	1.95
LiCl	1.5	0.4	0.6

https://doi.org/10.1021/acs.jpcc.6c00820
J. Phys. Chem. C XXXX, XXX, XXX−XXX

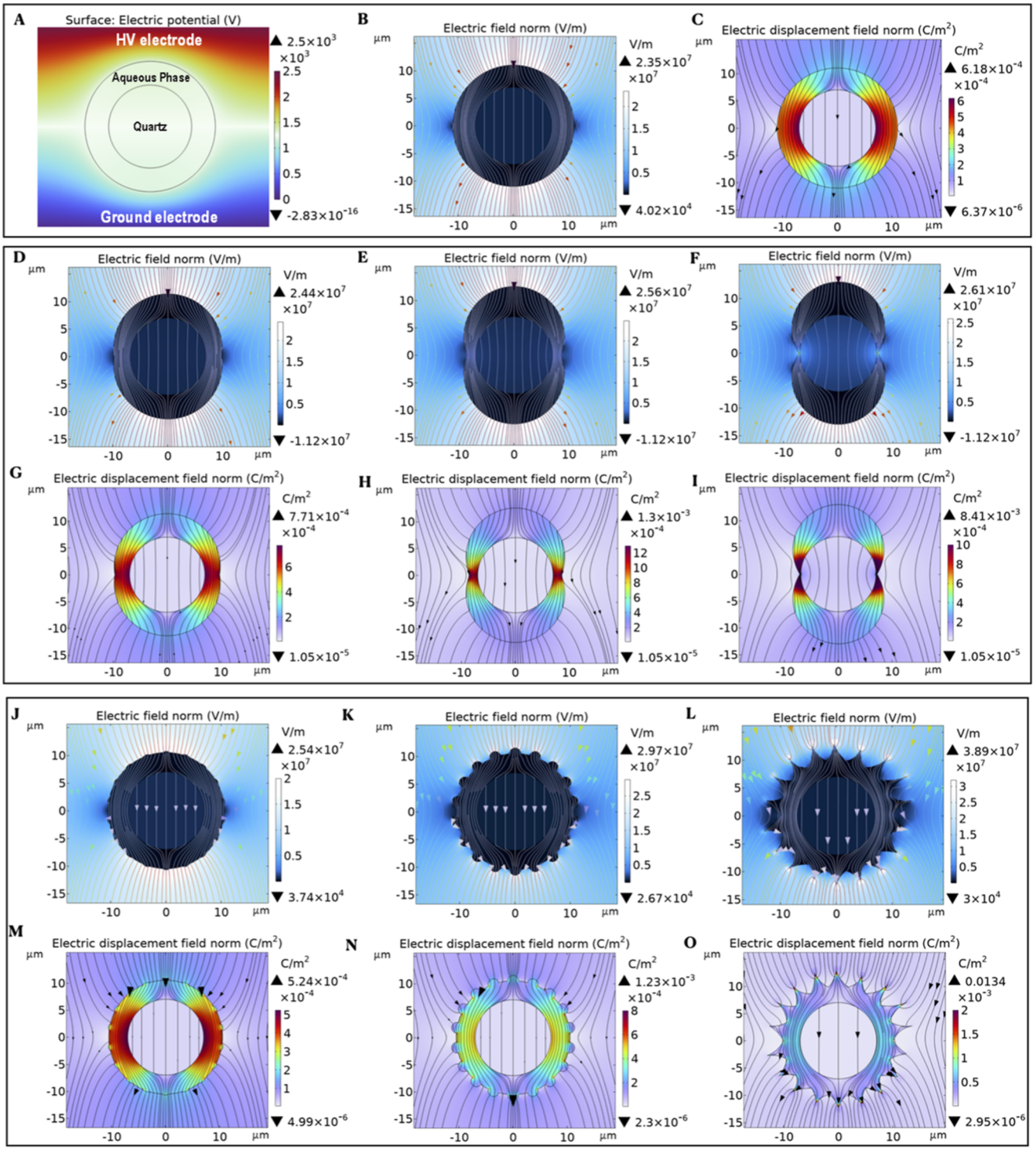

Figure 4. Schematic and field distribution analysis for a two-phase droplet system. (A) Electric potential distribution around the two-phase (quartz particle inside a water droplet) system. (B) Corresponding normal electric field distribution and (C) surface charge density on the initial neutral droplet; (D–F) electric field distribution on a neutral or low-conductivity water shell surrounding the quartz core as it evolves from its initial (D) to final deformed state; (F–H) corresponding electric displacement field distributions for the neutral or low-conductivity regime, showing initially uniform fields (G) transitioning to localized peaks at the horizontal poles (I). (J–L) Electric field distribution on an analogous high-conductivity case with enhanced ionic concentration as it evolves from its initial (J) to final deformed state; (L–N) corresponding electric displacement field distributions for the high-conductivity regime, showing initially uniform fields (M) transitioning to localized peaks at the sharp protrusions (O).

demonstrates approximately 85% energy saving in the case of LiCl. True specific energy consumption (J/mg SiO_2) is unavailable due to challenges in collecting larger quantities.

Anion Effects

In the next part of our experiments, we examined the influence of anions on quartz disintegration using sodium halides (NaF to NaI) at a fixed concentration of 0.1 ppm. TEM analyses (Figure

https://doi.org/10.1021/acs.jpcc.6c00820
J. Phys. Chem. C XXXX, XXX, XXX−XXX

3G−J) show that NaF, containing the low-polarizability F^- anion, exhibits the least efficiency, whereas NaCl, NaBr, and NaI produce progressively more monodisperse NPs and enhanced quartz breakdown as anion polarizability increases. Although NaI contributes fewer moles than NaF because of its higher molar mass, the larger and more polarizable I^- ion forms weaker hydration shells than F^- under these dilute conditions. This trend reflects the contrast between the strongly hydrogen-bonded, structured hydration environment of smaller anions (F^-) and the more weakly hydrated, flexible interfacial layer around the larger anions (I^-). The stronger hydration of smaller anions rigidifies the droplet interface, suppressing deformation and rapid charge redistribution, which stabilizes electrospray droplets and leads to incomplete mineral disintegration. Another key factor contributing to increasing anion polarizability shortens the charge relaxation length, thereby stabilizing the spray plume and maintaining stronger electric fields for effective Coulomb fission, independent of the total ion count. Taken together, these results demonstrate that ion-specific properties, such as hydration strength, polarizability, and mobility, have a critical influence on electrohydrodynamic processes in charged microdroplets. Informed selection of ion type thus offers a means to tune both the energy threshold for mineral disintegration and the morphology of NPs formed under ambient electrospray conditions.

Two primary factors control the electrohydrodynamics of aqueous salt droplets: the surface tension and electrical conductivity. Figure S5 shows how varying NaCl concentrations affects these properties. Even trace ionic impurities at ppm levels significantly increase the electrical conductivity of water while only slightly altering surface tension. A liquid droplet is held together by surface tension, which minimizes surface area and favors a spherical shape. When the droplet is electrically charged under an external field, Rayleigh instability governs its breakup at a critical point, influenced by parameters such as droplet diameter (D), charge relaxation time (τ), and charge relaxation length (d_m) (explained in detail later). Our experiments demonstrate that effective disintegration occurs only at low salt concentrations (0.1 ppm), which correlates with the region in Figure S6 where conductivity increases sharply without a corresponding significant change in surface tension. We therefore infer that droplet conductivity plays a key role in this phenomenon, which motivates the subsequent simulation study presented in the next section.

COMSOL Simulations

To illustrate how salt concentration modulates the electric field distribution, charge accumulation, and Maxwell stress within heterogeneous droplets, quasi-static COMSOL simulations were performed at representative snapshots of droplet evolution. These calculations resolve steady-state field geometries that contribute to the observed differences in fission modes but do not model the time-dependent growth of instability. Figure 4A illustrates a droplet containing an aqueous phase with a suspended quartz particle forming a two-phase system. In the current scenario, a dielectric (quartz), with relative permittivity (ε_r) = 4, surrounded by a layer of salt water, ε_r = 78−80, suspended in air with ε_r = 1, between a two-electrode system (not shown in the figure) was used. For the simulations, the quartz particle diameter was set to 5 μm, consistent with the experimentally measured particle size distribution (5−10 μm, Figure S1), while the nozzle diameter was set to 50 μm. During ejection, the quartz particle becomes encapsulated in a surrounding water layer, forming a composite droplet with a solid quartz core and a liquid shell. Depending on the thickness of this water layer, the effective radius of the composite droplet varies. To account for this variability, a droplet radius of 8−12 μm was incorporated into the COMSOL model to represent the realistic droplet size range observed during experiments. The top and bottom electrodes were at positive and ground potential, respectively. Figure 4B,C illustrates the electric field norm (V/m) distribution and the corresponding electric displacement field norm (C/m^2) representing charge density on the droplet, respectively. The direction of these vectors is indicated by streamlines (thin solid lines) and vectors (arrows), which originate from the positively charged electrode surface and terminate at the grounded surface. After setting up our simulated droplet system, we considered two scenarios: one at a low ($\leq$1.5 μM) and another at a high ($\geq$8.5 μM) salt concentration. Droplet sizes ($d_0 \approx 45-60$ μm) for aqueous cone-jet electrospray at flow rates of 0.1 mL h^{-1} and similar capillary geometries (ID 50 μm) have been extensively characterized in the literature and fall within this range.[19,20] Using these reported values together with our calculated charge relaxation lengths (Text S6.1), LiCl (d_m = 4.51 μm) gives $d_0/d_m \approx 10-13$, consistent with the rough fission regime (global deformation; Figure 4D−F), whereas NaCl (d_m = 1.59 μm) gives $d_0/d_m \approx 28-38$, favoring fine fission driven by localized surface instabilities (Figure 4J−O). Two factors determine the fate of the particle, namely, the electric field and the charge relaxation dynamics, which are discussed in detail in the next section of the manuscript.

Effect of the electric field: in the first case, when the drop acquires an electric charge under an externally applied electric field, it distributes on the surface, creating an outward Coulombic electrostatic force, as shown in Figure 4D−F. The image displays the magnitude of the electric field, represented by a color contour, with white denoting the highest strength and sapphire blue the lowest. Figure 4G−I shows the magnitude of the electric displacement field, represented by a color contour, where red denotes the highest strength and white the lowest. In the initial stable state (Figure 4G), the electric displacement field is quasi-uniform along the vertical poles of the droplet, exhibiting only mild distortion and a slight enhancement at the horizontal poles. These field distributions are consistent with conditions favoring the Rayleigh−Taylor-like instability growth, where electrostatic pressure exceeds capillary restoring force. Figure 4I shows that as the field becomes localized, the electric displacement field exhibits a highly dense region at the two horizontal extremities of the quartz particle. These regions represent high electric flux density, where large amounts of bound and free charges accumulate. Together with the previously reported chemically induced effects associated with reactive species (protons), the pronounced electric displacement at the poles produces an additional Maxwell electrostatic pressure at the solid−liquid interface.

These macroscopic electromechanical stresses at the solid−liquid interface likely contribute to weakening of the quartz lattice, complementing the chemically induced lattice slip mechanisms that ultimately lead to particle disintegration.

In the second case, where the salt concentration is high (5 ppm), Figure 4J−O illustrates enhanced conductivity in the outer water layer due to the added ionic concentration (NaCl). Here, the field lines are more densely packed at the top and bottom poles, indicating stronger polarization and field enhancement. This transition reflects how an increase in ionic

https://doi.org/10.1021/acs.jpcc.6c00820
J. Phys. Chem. C XXXX, XXX, XXX−XXX

concentration in water enhances charge screening and modifies field penetration. Figure 4J−L reveals the critical phenomenon, namely, electrostatic field enhancement. The electric and aerodynamic stresses induce instabilities akin to Rayleigh−Taylor and Kelvin−Helmholtz instabilities, leading to field localization. The electric field is no longer uniform around the droplet. Instead, it becomes highly concentrated at points of high surface curvature such as surface protrusions (Figure 4L). The color map vividly shows that the electric field is 1.5× higher at these protrusions than at the smoother, concave regions of the surface (Figure 4F). This is a direct consequence of the fact that surface charge density is highest at sharp points, a principle often referred to as the "lightning rod effect". Figure 4M−O demonstrates that the strong electric displacement field at these tips translates into significant Maxwell's electrostatic pressure, 562 kPa (shown in Figure S7), acting on the fluid surface, promoting localized stretching and potentially initiating oozing out of liquid from the droplet. Hence, the particle inside does not experience electrostatic pressure, unlike in the previous case, resulting in incomplete/poor disintegration of quartz.

Charge Relaxation Dynamics

The two cases of droplet fission described in the previous two paragraphs, which decide the fate of the quartz particle within, can be termed as "rough fission" (complete fragmentation of quartz) and "fine fission" (incomplete fragmentation of quartz).[20] At trace ionic concentrations, the electric field concentrates near the droplet poles, where localized charge accumulation enhances the electrostatic pressure. Increasing salt concentration to an optimum concentration strengthens this polarization, leading to intensified field focusing and asymmetric deformation of the droplets. Under low-conductivity conditions (where the added salt concentration is 0.1 ppm), charge relaxation within the droplets is relatively slow ($\tau = 2.36\ \mu s$) with a large charge relaxation length ($d_m = 4.51\ \mu m$). These parameters are explained in detail in Supporting Information S6.1. The externally applied electrostatic field induces Maxwell pressure (Figure 4D−F), acting outward and progressively amplifying surface deformation. Because of the low conductivity, charge carriers are relatively immobile. As the droplet deforms, charges cannot reorganize rapidly enough to concentrate on the newly forming regions of high curvature. Consequently, electrostatic stresses remain distributed approximately uniform over the surface. Instead of localized failure at a single point, the droplet becomes globally unstable (Figure 4D−F). When the perturbation amplitude approaches the limit of the droplet radius, it undergoes fission, inducing fragmentation into multiple large segments, often shattering embedded solid particles into nanosized subfragments.

In contrast, the conductivities are higher (where the added salt concentration is 0.5 ppm). Charge relaxation ($\tau = 0.69\ \mu s$) is much faster, and the relaxation length is smaller ($d_m = 1.59\ \mu m$). The minute disturbances correspond to the Kelvin−Helmholtz instability, triggered by interfacial velocity shear between the droplet and the surrounding air. Here, charge redistribution occurs rapidly, producing surface-bound perturbations rather than global deformation of the droplet. During this stage, the droplet's surface develops localized ripples that evolve into protrusions of high curvature (Figure 4J). Mobile surface charges rapidly redistribute toward regions of high surface curvature, leading to strong charge accumulation at the protrusion tips and pronounced amplification of the local electric field. The associated Maxwell electrostatic stress acts at the interface as an outward directed pressure that intensifies the deformation, while its tangential component, reaching magnitudes of approximately 125 kPa (Figure S7E,F), induces significant shear stresses along the aqueous phase surface. This combined action elongates surface protrusions into slender jets and overcomes the local capillary pressure at the tip, resulting in the formation of a sharp Taylor cone from which a thin, highly charged liquid jet is emitted.[21,22] The emitted jet subsequently undergoes capillary breakup, producing small, relatively monodispersed daughter droplets. This fission mode, commonly referred to as fine fission, is characterized by the transient formation of Taylor cones and repeated microjet ejection events.[22,23] In contrast to rough fission, fine fission does not lead to complete fragmentation of the quartz particles encapsulated within the droplet; instead, it preferentially expels water-rich layers as fine droplets through successive emission cycles. A detailed description of this phenomenon, together with a schematic flow diagram elucidating the physical mechanisms governing the breakup behavior of quartz particles encapsulated within water droplets of varying conductivity and ejected from a high-voltage nozzle, is provided in Supporting Information, Figure S8. These observations indicate that the breakup dynamics are governed by the ratio between the droplet diameter and the charge relaxation length (d_m).[24] Specifically, when $d \gg d_m$ breakup proceeds via fine fission driven by localized surface instabilities, global droplet deformation dominates, leading to rough fission.

CONCLUSIONS

This study demonstrates a tunable regime in charged water microdroplet-mediated disintegration of natural minerals, where ionic concentration, type, and size critically determine NP size, morphology, and uniformity. We find that proton- and lithium-ion-assisted cleavage mechanisms offer the lowest energy pathways, significantly reducing the applied potential threshold for quartz disintegration by up to 85%, with NPs as small as 2−10 nm formed at voltages as low as 1.5 kV. COMSOL simulations reveal that the applied electric field causes charge accumulation and electric field localization at the droplet poles, initiating deformation. At low conductivity, delayed charge relaxation enhances the amplitude of surface perturbations until they grow to a size comparable to the droplet radius, a characteristic of the Rayleigh−Taylor instability, leading to catastrophic breakup. In contrast, under high conductivity, charge redistribution is rapid, and perturbations manifest as small ripples or corrugations driven by Kelvin−Helmholtz instability. The resulting tangential Maxwell stresses induce localized shear and fine jets. Together, experiments and simulations show that salt-assisted electrospray enhances mineral disintegration in charged water microdroplets by providing additional electrostatic pressure, alongside proton-induced slip, thereby lowering the required potential compared with pure water. This approach provides a green and scalable platform for controlled nanomaterial synthesis. By highlighting the fundamental role of ions in sculpting microdroplet electrohydrodynamics and reaction pathways, this work opens new avenues for ion-engineered microreactor technologies. Such advances pave the way for the sustainable synthesis of functional NPs from natural minerals with exceptional energy efficiency and morphological control, expanding the applicability of microdroplet chemistry in catalysis, environmental remediation, and materials science.

https://doi.org/10.1021/acs.jpcc.6c00820
J. Phys. Chem. C XXXX, XXX, XXX−XXX

■ ASSOCIATED CONTENT

Data Availability Statement

The data supporting this article are included in the main article and its Supporting Information. No additional data have been deposited in external repositories.

Supporting Information

The Supporting Information is available free of charge at https://pubs.acs.org/doi/10.1021/acs.jpcc.6c00820.

Materials, experimental methods, and additional results and discussion (PDF)

■ AUTHOR INFORMATION

Corresponding Authors

Depanjan Sarkar − *DST Unit of Nanoscience (DST UNS) & Thematic Unit of Excellence (TUE), Department of Chemistry, Indian Institute of Technology Madras (IITM), Chennai 600036, India; Centre of Excellence on Molecular Materials and Functions, Department of Chemistry, Indian Institute of Technology Madras, Chennai 600036, India*; Email: depanjan_coe@icsrpis.iitm.ac.in

Thalappil Pradeep − *DST Unit of Nanoscience (DST UNS) & Thematic Unit of Excellence (TUE), Department of Chemistry, Indian Institute of Technology Madras (IITM), Chennai 600036, India; International Centre for Clean Water, 2nd Floor, B-Block, IIT Madras Research Park, Chennai 600113, India; Centre of Excellence on Molecular Materials and Functions, Department of Chemistry, Indian Institute of Technology Madras, Chennai 600036, India*; orcid.org/0000-0003-3174-534X; Email: pradeep@iitm.ac.in

Authors

Jamshiya Sulthana − *DST Unit of Nanoscience (DST UNS) & Thematic Unit of Excellence (TUE), Department of Chemistry, Indian Institute of Technology Madras (IITM), Chennai 600036, India*

Anubhav Mahapatra − *DST Unit of Nanoscience (DST UNS) & Thematic Unit of Excellence (TUE), Department of Chemistry, Indian Institute of Technology Madras (IITM), Chennai 600036, India*; orcid.org/0009-0002-1262-2598

Mridula Bhan − *DST Unit of Nanoscience (DST UNS) & Thematic Unit of Excellence (TUE), Department of Chemistry, Indian Institute of Technology Madras (IITM), Chennai 600036, India*

Complete contact information is available at: https://pubs.acs.org/10.1021/acs.jpcc.6c00820

Author Contributions

‖J.S. and A.M. contributed equally to the work. J.S. and A.M.: data collection, data analysis, data interpretation, and writing the manuscript. M.B.: COMSOL simulations and writing the manuscript. D.S.: conception and design of work, supervision of data collection and analysis, interpretation of results, drafting and editing of the article. T.P.: conception, supervision of data analysis, interpretation of results, and editing of the final version of the article.

Notes

The authors declare the following competing financial interest(s): Indian patent IN202441104922 for the method of efficient transformation of crystalline minerals to nanoparticles by salt-containing microdroplets was published on December 17, 2025. J.S., A.M., D.S., and T.P. are listed as inventors. The invention discloses an electrospray method and applications, which are correlated with the research reported here.

■ ACKNOWLEDGMENTS

The authors gratefully acknowledge financial support from the Anusandhan National Research Foundation (ANRF), Department of Science and Technology (DST), University Grants Commission (UGC), Centre for Industrial Consultancy and Sponsored Research (IC&SR), and Government of India through the Institution of Eminence Scheme of IIT Madras (Centre of Excellence on Molecular Materials and Functions). The transmission electron microscopy (TEM) measurements were performed and analyzed at the ANRF National Facility for Cryo-Electron Microscopy, IIT Madras.

■ REFERENCES

(1) Aramendia, E.; Brockway, P. E.; Taylor, P. G.; Norman, J. Global Energy Consumption of the Mineral Mining Industry: Exploring the Historical Perspective and Future Pathways to 2060. *Glob. Environ. Change* **2023**, *83*, 102745.

(2) Norgate, T.; Haque, N. Energy and Greenhouse Gas Impacts of Mining and Mineral Processing Operations. *J. Cleaner Prod.* **2010**, *18* (3), 266−274.

(3) Raabe, D. The Materials Science behind Sustainable Metals and Alloys. *Chem. Rev.* **2023**, *123* (5), 2436−2608.

(4) Lee, J. K.; Banerjee, S.; Nam, H. G.; Zare, R. N. Acceleration of Reaction in Charged Microdroplets. *Q. Rev. Biophys.* **2015**, *48* (4), 437−444.

(5) Holden, D. T.; Shira, B. A.; Edwards, M. Q.; Morato, N. M.; Cooks, R. G. Mechanisms of Ionization and of Chemical Reactions in Charged Microdroplets. *Chem. Sci.* **2025**, *16* (37), 17020−17033.

(6) Yan, X. Emerging Microdroplet Chemistry for Synthesis and Analysis. *Int. J. Mass Spectrom.* **2021**, *468*, 116639.

(7) Xiong, H.; Lee, J. K.; Zare, R. N.; Min, W. Strong Electric Field Observed at the Interface of Aqueous Microdroplets. *J. Phys. Chem. Lett.* **2020**, *11* (17), 7423−7428.

(8) Rovelli, G.; Jacobs, M. I.; Willis, M. D.; Rapf, R. J.; Prophet, A. M.; Wilson, K. R. A Critical Analysis of Electrospray Techniques for the Determination of Accelerated Rates and Mechanisms of Chemical Reactions in Droplets. *Chem. Sci.* **2020**, *11* (48), 13026−13043.

(9) Layman, B. R.; Hill, M. L.; Dick, J. E. Radical Electroprecipitation Prolongs "Electro"Chemiluminescence of the Tris(2,2'-Bipyridyl)-Ruthenium(II) and Tri- *n* -Propylamine System by a Millionfold. *J. Am. Chem. Soc.* **2026**, *148* (4), 4206−4216.

(10) Sarkar, D.; Mahitha, M. K.; Som, A.; Li, A.; Wleklinski, M.; Cooks, R. G.; Pradeep, T. Metallic Nanobrushes Made Using Ambient Droplet Sprays. *Adv. Mater.* **2016**, *28* (11), 2223−2228.

(11) Unni, K.; Shantha Kumar, J.; Som, A.; Sarkar, D.; Pradeep, T. From Solution to Microstructures in Minutes: Microdroplet-Derived Stand-Alone TiO_2 Surfaces for Simultaneous Water Harvesting and Treatment. *ACS Sustainable Chem. Eng.* **2024**, *12* (32), 11957−11967.

(12) Li, A.; Luo, Q.; Park, S.; Cooks, R. G. Synthesis and Catalytic Reactions of Nanoparticles Formed by Electrospray Ionization of Coinage Metals. *Angew. Chem., Int. Ed.* **2014**, *53* (12), 3147−3150.

(13) Li, A.; Baird, Z.; Bag, S.; Sarkar, D.; Prabhath, A.; Pradeep, T.; Cooks, R. G. Using Ambient Ion Beams to Write Nanostructured Patterns for Surface Enhanced Raman Spectroscopy. *Angew. Chem., Int. Ed.* **2014**, *53* (46), 12528−12531.

(14) Sarkar, D.; Singh, R.; Som, A.; Manju, C. K.; Ganayee, M. A.; Adhikari, R.; Pradeep, T. Electrohydrodynamic Assembly of Ambient Ion-Derived Nanoparticles to Nanosheets at Liquid Surfaces. *J. Phys. Chem. C* **2018**, *122* (31), 17777−17783.

(15) Spoorthi, B. K.; Debnath, K.; Basuri, P.; Nagar, A.; Waghmare, U. V.; Pradeep, T. Spontaneous Weathering of Natural Minerals in Charged Water Microdroplets Forms Nanomaterials. *Science* **2024**, *384* (6699), 1012−1017.

(16) Mahapatra, A.; Som, A.; Spoorthi, B. K.; Sarkar, D.; Pradeep, T. From Micro-to-Nano in Charged Water Microdroplets: Unveiling Steps in the Weathering of Minerals. *Chem. Commun.* **2025**, *61* (81), 15846−15849.
(17) Pradeep, T. Microdroplet Mechanochemistry. *ACS Sustainable Chem. Eng.* **2026**, *14* (1), 25−30.
(18) Chen, W.; Liu, J.; Jiang, Q.; Wang, N.; Wu, X.; Xia, D.; He, G.; Francisco, J. S. Silica-Driven CO_2 Reduction in Water Microdroplets. *J. Am. Chem. Soc.* **2025**, *147* (29), 25287−25294.
(19) Gañán-Calvo, A. M.; Dávila, J.; Barrero, A. Current and Droplet Size in the Electrospraying of Liquids. Scaling Laws. *J. Aerosol Sci.* **1997**, *28* (2), 249−275.
(20) Kim, J. Y.; Lee, S. J.; Hong, J. G. Spray Mode and Monodisperse Droplet Properties of an Electrospray. *ACS Omega* **2022**, *7* (32), 28667−28674.
(21) Fernández De La Mora, J. On the Outcome of the Coulombic Fission of a Charged Isolated Drop. *J. Colloid Interface Sci.* **1996**, *178* (1), 209−218.
(22) Avadhani, V. S.; Harper, C. C.; Miller, Z. M.; Williams, E. R. Spontaneous Fission of Charged Water Nanodrops: Unveiling the Stochastic Nature of Fission Pathways and Dynamics. *J. Am. Chem. Soc.* **2025**, *147* (22), 18853−18863.
(23) Consta, S. Atomistic Modeling of Jet Formation in Charged Droplets. *J. Phys. Chem. B* **2022**, *126* (41), 8350−8357.
(24) Marginean, I.; Znamenskiy, V.; Vertes, A. Charge Reduction in Electrosprays: Slender Nanojets as Intermediates. *J. Phys. Chem. B* **2006**, *110* (12), 6397−6404.

https://doi.org/10.1021/acs.jpcc.6c00820
J. Phys. Chem. C XXXX, XXX, XXX−XXX